Chandrika P. Vyasarayani[1]
e-mail: cpvyasar@engmail.uwaterloo.ca

Eihab M. Abdel-Rahman

John McPhee

Stephen Birkett

Systems Design Engineering,
University of Waterloo,
Waterloo, ON, N2L 3G1, Canada

Modeling MEMS Resonators Past Pull-In

In this paper, we develop a mathematical model of an electrostatic MEMS (Micro-Electro-Mechanical systems) beam undergoing impact with a stationary electrode subsequent to pull-in. We model the contact between the beam and the substrate using a nonlinear foundation of springs and dampers. The system partial differential equation is converted into coupled nonlinear ordinary differential equations using the Galerkin method. A numerical solution is obtained by treating all nonlinear terms as external forces. We use the model to predict the contact length, natural frequencies, and mode shapes of the beam past pull-in voltage as well as the dynamic response of a shunt switch in a closing and opening sequence.
[DOI: 10.1115/1.4002835]

1 Introduction

Stiction failures are now posing a significant challenge to the commercial deployment of RF (Radio Frequency) MEMS switches. The prevalence of these failures has undermined the reliability of MEMS switches. In these failures, the switch structure deforms to contact the substrate in response to an actuation voltage beyond the pull-in threshold. When the actuation signal is removed completely, the switch fails to come back to its flat (equilibrium) position due to the surface forces between the structure and the substrate.

A large body of work has been lately dedicated to modeling the motions of MEMS up to pull-in [1,2]. Gupta et al. [3] conducted experiments and simulations on the transient dynamics of a microbeam driven by a dc voltage at varying ramp-rates. They showed that the microbeam can pull-in at voltages below the statically calculated pull-in voltage because of the transient effects of the ramp-rate. Nielson and Barbastathis [4], using a lumped-mass model of a parallel-plate actuator, found that pull-in occurs at half the electrostatic gap. The associated bifurcation was assumed to be the dynamic pull-in where the voltage was only 91.1% of the static pull-in voltage. A similar conclusion was drawn by Fargas-Marquès and Shkel [5] based on a lumped-mass model and later verified experimentally [6]. In their case, a dynamic pull-in voltage was defined as the maximum step-voltage that can be applied to the system without leading to the collapse of the upper electrode. Elata and Bamberger [7] generated a stagnation curve that characterizes all those deflection states where an applied voltage can bring the microbeam to rest. Similar to the lumped-mass models listed above, this curve predicted a dynamic pull-in voltage at 91% of the static pull-in voltage. Nayfeh and co-workers [2,8] generated frequency-response curves describing the resonant response of a clamped-clamped electrostatic microbeam. They showed that dynamic pull-in can occur under combinations of dc and ac voltages as low as 25% of the static pull-in voltage, whenever the frequency of the ac component is in the neighborhood of a resonant frequency [1].

Research on modeling the behavior of MEMS past pull-in has been scarce. Savkar and Murphy [9,10] and Savkar et al. [11] proposed a vibratory release mechanism for stiction-failed beams, where an ac voltage, tuned to a resonance of the beam, is applied to the release of the beam. In their work, they assume the contact length of the beam and the substrate. The frequency at which the beam should be driven must correspond to a favorable mode shape that will facilitate debonding of the beam from the substrate. Gorthi et al. [12] studied the past pull-in behavior of cantilever microbeams. They obtained the static deflections and their stability for different dc voltages and dielectric layer thickness.

Models of MEMS past pull are useful in analyzing MEMS impact actuators such as that proposed by Bienstman et al. [13]. These actuators are designed to undergo repeated impacts in the course of their operation. They can also be used to model the opening and closing of series and shunt switches to study switching time, contact force, and contact bounce (rattling) events. Another important use of past pull-in MEMS models is to enable the investigation of stiction failures and the surface forces causing them and to design systems to repair stiction-failed MEMS.

A simpler release mechanism could envisage using a mobile electrode to apply a dc voltage drop on the other side of a stiction-failed MEMS. The magnitude of the applied voltage is a function of adhesion energy between a failed beam and the substrate, which is directly linked to the contact length of the beam and substrate. Therefore, the estimation of the contact length, natural frequencies, and mode shapes of the beam while in contact with the substrate is essential. In this work we develop a mathematical model to predict the contact length, natural frequencies, and mode shapes of the beam past pull-in voltage as well as the dynamic response of a shunt switch in a closing and opening sequence.

2 Mathematical Model

We consider an electrostatically actuated fixed-fixed microbeam (Fig. 1). A voltage drop $V(t)$ is applied between the beam and an overlapping electrode underneath it. A dielectric layer (d_2-d_1) thick is fabricated on top of the electrode to protect against short-circuit during impact. As a result, impact occurs when the beam deflection $w(x,t)$ exceeds the air gap d_1, while the beam has yet to close the capacitor gap d_2.

We use the Euler–Bernoulli beam theory, include the effects of the geometrical nonlinearity arising from midplane stretching as well as the impact of the microbeam on the substrate, and write the microbeam equation of motion as follows:

$$EI\frac{\partial^4 w}{\partial x^4} + \rho A\frac{\partial^2 w}{\partial t^2} + c\frac{\partial w}{\partial t} = \left[\frac{EA}{2L}\int_0^L\left(\frac{\partial w}{\partial x}\right)^2 dx + P\right]\frac{\partial^2 w}{\partial x^2} + \frac{\epsilon b V^2(t)}{2(d_2-w)^2} - F_c(x,t) \tag{1}$$

where EI is the flexural rigidity, ρA is the mass per unit length, c is the coefficient of viscous damping per unit length, b and L are

[1]Corresponding author.

Contributed by the Design Engineering Division of ASME for publication in the Journal of Computational and Nonlinear Dynamics. Manuscript received August 30, 2009; final manuscript received October 9, 2010; published online February 1, 2011. Assoc. Editor: Albert C. J. Luo.

Copyright © 2011 by ASME

Downloaded From: http://computationalnonlinear.asmedigitalcollection.asme.org/ on 03/17/2013 Terms of Use: http://asme.org/terms

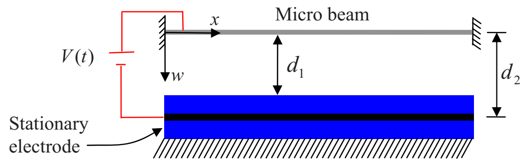

Fig. 1 Fixed-fixed MEMS beam

the beam width and length, P is the axial tensile load, ϵ is the permittivity of the capacitor medium, and $F_c(x,t)$ is the contact force applied at the locations where the beam is in contact with the substrate. The boundary conditions of Eq. (1) are

$$w(0,t) = w(L,t) = 0 \quad \text{and} \quad \left.\frac{\partial w}{\partial x}\right|_{(0,t)} = \left.\frac{\partial w}{\partial x}\right|_{(L,t)} = 0 \tag{2}$$

One way to simulate contact is to model the substrate as an elastic foundation model: a continuum of springs that can only react in compression. When the beam comes into contact with the substrate, a contact force is generated due the deformation of the foundation springs. If we use sufficiently stiff foundation springs, the deformation in the substrate will be minimal. In the limit, when the stiffness of the foundation springs approach infinity, it will result in zero deformation representing the case of rigid contact. The deformation of the foundation due to finite stiffness represents the cumulative local deformations in the thickness of the beam and the substrate. The force-compression relation of two contacting bodies is usually nonlinear in nature due to the geometry of the contacting surfaces and due to local plastic deformations in microscopic contact regions; thus, a nonlinear foundation of springs captures the contact behavior more accurately. Figure 2 shows the foundation model of the substrate.

We define a gap function $g(x,t)=w(x,t)-d_1$, which is positive at locations where there is contact and negative where there is no contact. Assuming the nonlinear force-compression relation $F_c = k_c\Delta^n$, where Δ is the deformation, the distributed contact force can now be written as

$$F_c(x,t) = k_c g(x,t)^n H(g(x,t)) \tag{3}$$

In the above expression, the Heaviside function $H(g(x,t))$ ensures that contact force is applied only at those locations where the deformation $g(x,t)$ is positive.

Impact is always associated with energy losses [14] due to the plastic deformations in the contact region, excitation of vibrational modes in the substrate, and generation of sound and heat. Equation (3) can be modified to account for these energy losses. Several damping models like linear, nonlinear, and deformation-dependent damping models are used in literature to simulate the impact damping [14]. Deformation dependent damping is widely used to simulate impact losses, since it results in a continuous impact force [15–17]. In this model, the force-deformation relation is given by $F_c = k_c\Delta^n + \mu\Delta^n\dot{\Delta}$. Since the damping force is dependent on the deformation, the contact force at the beginning and end of contact is zero. Including the damping term in Eq. (3), we get

$$F_c(x,t) = k_c g(x,t)^n\left(1 + \mu\frac{\partial g}{\partial t}\right)H(g(x,t)) \tag{4}$$

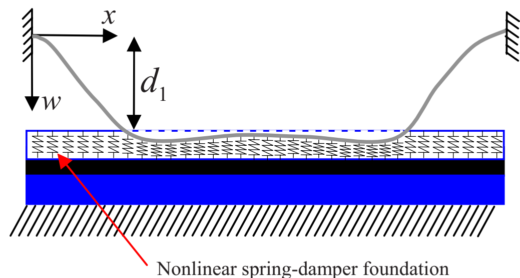

Fig. 2 Foundation model of the substrate

We introduce the following nondimensional parameters into the equation of motion:

$$\hat{x} = \frac{x}{L}, \quad \hat{w} = \frac{w}{d_1}, \quad \beta = \frac{d_1}{d_2}, \quad \alpha_1 = 6\left(\frac{d_1}{h}\right)^2, \quad \hat{t} = \frac{t}{T}, \quad \hat{c} = \frac{cL^4}{EIT}$$

$$\hat{\mu} = \frac{\mu d_1}{T}, \quad \alpha_2 = \frac{6\epsilon L^4}{Eh^3 d_1 d_2^2}, \quad \hat{k}_c = \frac{k_c L^4 d_1^{n-1}}{EI}, \quad \text{and} \quad \hat{P} = \frac{PL^2}{EI} \tag{5}$$

where the time scale T is defined as $T=\sqrt{(\rho A L^4/EI)}$. The resulting nondimensional equation of motion, after dropping the circumflexes for clarity, is

$$\frac{\partial^4 w}{\partial x^4} + \frac{\partial^2 w}{\partial t^2} + c\frac{\partial w}{\partial t} = \left[\alpha_1\int_0^1\left(\frac{\partial w}{\partial x}\right)^2 dx + P\right]\frac{\partial^2 w}{\partial x^2} + \frac{\alpha_2 V^2(t)}{(1-\beta w)^2} - k_c g(x,t)^n\left(1 + \mu\frac{\partial g}{\partial t}\right)H(g(x,t)) \tag{6}$$

with the boundary conditions

$$w(0,t) = w(1,t) = 0 \quad \text{and} \quad \left.\frac{\partial w}{\partial x}\right|_{(0,t)} = \left.\frac{\partial w}{\partial x}\right|_{(1,t)} = 0 \tag{7}$$

Equations (6) and (7) constitute the complete system model.

2.1 Solution Procedure. We use the Galerkin method to convert Eq. (6) into a system of nonlinear differential equations [18]. Therefore, we assume the solution to Eq. (6) is of the following form:

$$w(x,t) = \sum_{j=1}^{N}\phi_j(x)\eta_j(t) \tag{8}$$

where η_j are the generalized coordinates and $\phi_j(x)$ are the basis functions of the Galerkin reduction. We use the undamped mode shapes of a fixed-fixed beam without axial tension as basis functions. Since the electrostatic field applied on the beam and the supports are symmetric about the midpoint of the beam, we will only consider modes that are symmetric about midpoint in the Galerkin expansion. The closed-form expressions for mode shapes $\phi_j(x)$ are given by

$$\phi_j(x) = \sinh(\beta_j x) - \sin(\beta_j x) + \frac{\sinh(\beta_j) - \sin(\beta_j)}{\cosh(\beta_j) - \cos(\beta_j)}[\cosh(\beta_j x) - \cos(\beta_j x)] \tag{9}$$

The values of β_j are obtained by solving the following characteristic equation:

$$\cos(\beta_j)\cosh(\beta_j) - 1 = 0 \tag{10}$$

After substituting Eq. (8) into Eq. (6), we multiply the resulting equation with $\phi_k(x)$ and integrate over the domain. Making use of the orthogonality of the mode shapes, the following N second-order coupled nonlinear differential equations are obtained:

Downloaded From: http://computationalnonlinear.asmedigitalcollection.asme.org/ on 03/17/2013 Terms of Use: http://asme.org/terms

$$
\begin{aligned}
&\ddot{\eta}_k + 2\zeta_k\omega_k\dot{\eta}_k + \omega_k^2\eta_k \\
&= \alpha_2 V^2(t)\int_0^1 \frac{\phi_k(x)}{\left(1-\beta\sum_{j=1}^{N}\phi_j(x)\eta_j\right)^2}dx \\
&+ \left[\alpha_1\int_0^1\left(\sum_{j=1}^{N}\phi_j'(x)\eta_j\right)^2 dx + P\right]\sum_{j=1}^{N}\eta_j\int_0^1\phi_j''(x)\phi_k(x)dx \\
&- k_c\int_0^1\left(\sum_{j=1}^{N}\phi_j(x)\eta_j - 1\right)^n\left[1+\mu\left(\sum_{j=1}^{N}\phi_j(x)\dot{\eta}_j\right)\right] \\
&\times H(g(x,t))\phi_k(x)dx \quad k=1,2,\ldots,N
\end{aligned} \tag{11}
$$

where $\omega_k=\beta_k^2$ and ζ_k are the modal damping ratios. Once the system parameters have been specified, Eq. (11) can be numerically integrated to obtain the time evolution of the modal coordinates.

2.2 Linearized Model. In order to predict the natural frequencies and mode shapes, we linearize the partial differential equation (Eq. (6)) about the static equilibrium. The beam assumes different static equilibrium positions at different voltages. Let $w_e(x)$ be the equilibrium position of the beam under a dc voltage $V(t)=V_{\mathrm{dc}}$ and $u(x,t)$ be a small motion around the equilibrium position. We substitute the transformation

$$
w(x,t) = w_e(x) + u(x,t) \tag{12}
$$

in the equation of motion and drop terms nonlinear in u, the damping terms, and the terms representing the static equilibrium, to obtain the linearized equation of motion

$$
\begin{aligned}
\frac{\partial^4 u}{\partial x^4} + \frac{\partial^2 u}{\partial t^2} &= \left[\alpha_1\int_0^1\left(\frac{\partial w_e}{\partial x}\right)^2 dx + P\right]\frac{\partial^2 u}{\partial x^2} \\
&+ \left[2\alpha_1\int_0^1\frac{\partial w_e}{\partial x}\frac{\partial u}{\partial x}dx\right]\frac{\partial^2 w_e}{\partial x^2} + \frac{2\alpha_2 V_{\mathrm{dc}}^2}{(1-\beta w_e)^3}u \\
&- [k_c n(w_e-1)^{n-1}H(w_e-1)]u
\end{aligned} \tag{13}
$$

Identical boundary conditions to those shown in Eq. (7) apply to u.

Since Eq. (13) is an integro-partial differential equation, the method of separation of variables cannot be used to obtain the eigenvalue problem, so we use the Galerkin expansion to approximate the natural frequencies and mode shapes. We assume a solution to Eq. (13) of the form

$$
u(x,t) = \sum_{j=1}^{N}\phi_j(x)r_j(t) \tag{14}
$$

Substituting this solution in Eq. (13) and carrying out the Galerkin reduction, we obtain a set of coupled linear ordinary differential equations

$$
\begin{aligned}
&\ddot{r}_k + \omega_k^2 r_k - 2\alpha_2\beta V_{\mathrm{dc}}\sum_{j=1}^{N} r_j\int_0^1\frac{\phi_j(x)\phi_k(x)}{(1-\beta w_e)^3}dx \\
&- \left[\alpha_1\int_0^1\left(\frac{\partial w_e}{\partial x}\right)^2 dx + P\right]\sum_{j=1}^{N} r_j\int_0^1\phi_j''(x)\phi_k(x)dx \\
&- 2\alpha_1\left[\sum_{j=1}^{N} r_j\int_0^1\frac{\partial w_e}{\partial x}\phi_j'(x)dx\right]\int_0^1\frac{\partial^2 w_e}{\partial x^2}\phi_k(x)dx \\
&+ k_c n\sum_{j=1}^{N} r_j\int_0^1(w_e-1)^{n-1}H(w_e-1)\phi_j(x)\phi_k(x)dx = 0
\end{aligned}
$$

$$
k=1,2,\ldots,N \tag{15}
$$

Equation (15) can be rearranged into the matrix form

$$
\mathbf{I}\ddot{\mathbf{r}} + \mathbf{K}\mathbf{r} = \mathbf{0} \tag{16}
$$

The eigenvalues and eigenvectors of this discrete linear system can now be evaluated. The eigenvalues of the discrete system approximate the natural frequencies Ω_k of the beam in-flight and in contact with the substrate (before and after pull-in). The kth mode shape of the beam can now be obtained as

$$
U_k(x) = \sum_{j=1}^{N}\phi_j(x)r_j^k \tag{17}
$$

where r^k is the kth mode of the discrete system.

Table 1 Micro-actuator parameters

b	100 μm
d_1	1.18 μm
d_2	1.24 μm
E	166 GPa
ρ	2332 kg/m^3
h	1.5 μm
L	210 μm
N	0.0009 N
k_c	4.7×10^{11}
ϵ	8.854×10^{-12} F/m
n	3
α_1	3.713
α_2	0.106
P	8.501
μ	0.8
ζ_j	0.6

3 Results and Discussion

In this section we present numerical results obtained using our model. Initially, we validate the model, and then we present the convergence analysis of the static equilibrium. We then discuss how natural frequencies and mode shapes of the beam change with the applied dc voltage while in contact with the substrate. Finally, we use our model to simulate the entire range of motion of a shunt switch as it closes and opens.

3.1 Model Validation. Equation (11) was numerically integrated in MATLAB using the integrator ODE15S for an electrostatic micro-actuator with the dimensions and properties shown in Table 1. To obtain the equilibrium configuration of the beam for a given voltage V_{dc}, we integrate Eq. (11) for a long time until the system response settled to an equilibrium configuration. The equilibrium configuration was then substituted into Eq. (16) and the eigenvalue analysis was carried out to evaluate the natural frequencies and mode shapes of the beam in-flight. Figure 3 shows the natural frequencies of the beam, at different voltages.

To validate our model, we compare our results up to pull-in, assuming no dielectric layer $\beta=1$, to those obtained experimentally by Legtenberg and Tilmans [19] for an actuator with the same specifications. It can be seen from the figure that there is a good match between the results predicted by our analytical model and those they obtained experimentally. The natural frequency of the beam eventually drops to zero at a critical voltage known as pull-in. Beyond the pull-in voltage, the beam contacts the substrate.

3.2 Convergence Analysis. Younis et al. showed [2] that five symmetric modes are sufficient to capture the behavior of the beam in-flight. Those results do not apply while the beam is in contact with the substrate. We included higher-order modes to conduct the convergence analysis of the eigenvalue problem for

Downloaded From: http://computationalnonlinear.asmedigitalcollection.asme.org/ on 03/17/2013 Terms of Use: http://asme.org/terms

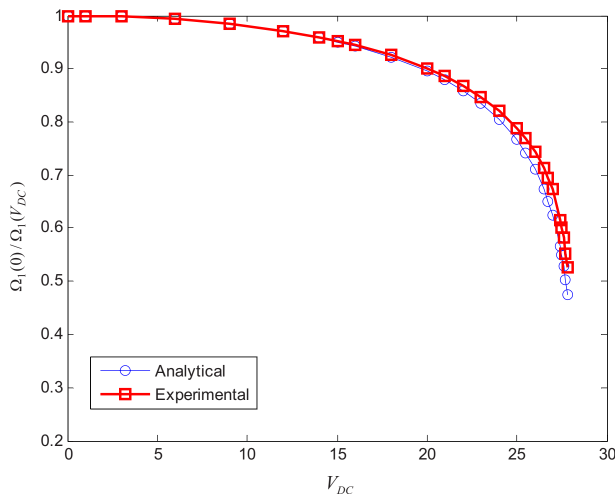

Fig. 3 Comparison of the natural frequencies obtained analytically and experimentally [19]. $\Omega_1(V_{dc})$ is the fundamental natural frequency of the beam as a function of dc voltage and $\Omega_1(0)$ is the frequency at $V_{dc}=0$. The results are for $\beta=1$ consistent with the experimental system [19].

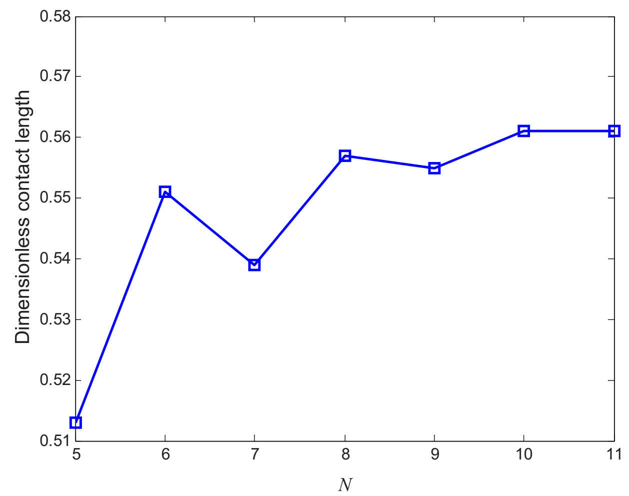

Fig. 5 Contact length using 5-mode to 11-mode approximations

the beam in contact. However, the closed-form representation of the modes shapes (Eq. (9)) suffers from numerical instability for modes higher than the fifth symmetric mode. Figure 4(*a*) shows the fifth to tenth symmetric modes of the fixed-fixed beam obtained by evaluating Eq. (9). The higher mode shapes are distorted over progressively longer stretches from the right support ($x=1$). This is due to the interaction of the machine noise with the hyperbolic functions used in the mode shape representation.

Gonçalves et al. [20] observed this numerical instability in the evaluation of higher-order modes and proposed an alternative representation of the mode shapes that is numerically more stable. We propose another method to overcome this instability. We mirror the left-half of the mode shape (from the left support to the midpoint) and use that image to represent the right-half of the mode shape (from the midpoint to the right support). This method can be used to reconstruct higher-order symmetric and antisymmetric modes as long as the numerical instability does not grow enough to approach the midpoint of the beam. Figure 4(*b*) shows the higher-order modes obtained using this method.

Figure 5 shows the contact length of the beam at a voltage of $V_{dc}=60$ V as the number of modes is increased. The difference in the contact length between the 10-mode and 11-mode is 6×10^{-4}. The static deflection of the beam using 5-mode, 10-mode, and 11-mode approximations is shown in Fig. 6. The 10-mode and 11-mode configurations are indistinguishable indicating convergence.

We conclude from the convergence study that at least 10-mode shapes should be retained in the models of beams in contact. The flat configuration of the beam midsection, while in contact with the substrate, is the reason for the recruitment of higher-order modes in the Galerkin expansion. This configuration imposes large strains and stores strain energy in the beam, thereby requiring the participation of the more energetic higher-order modes. Geometrically, it can be seen that representing the straight line of the contact section requires a larger number of the smooth mode shapes functions. In this analysis, the contact stiffness k_c was chosen sufficiently high such that the maximum penetration of the beam into the substrate was kept less than 1% of the beam thickness.

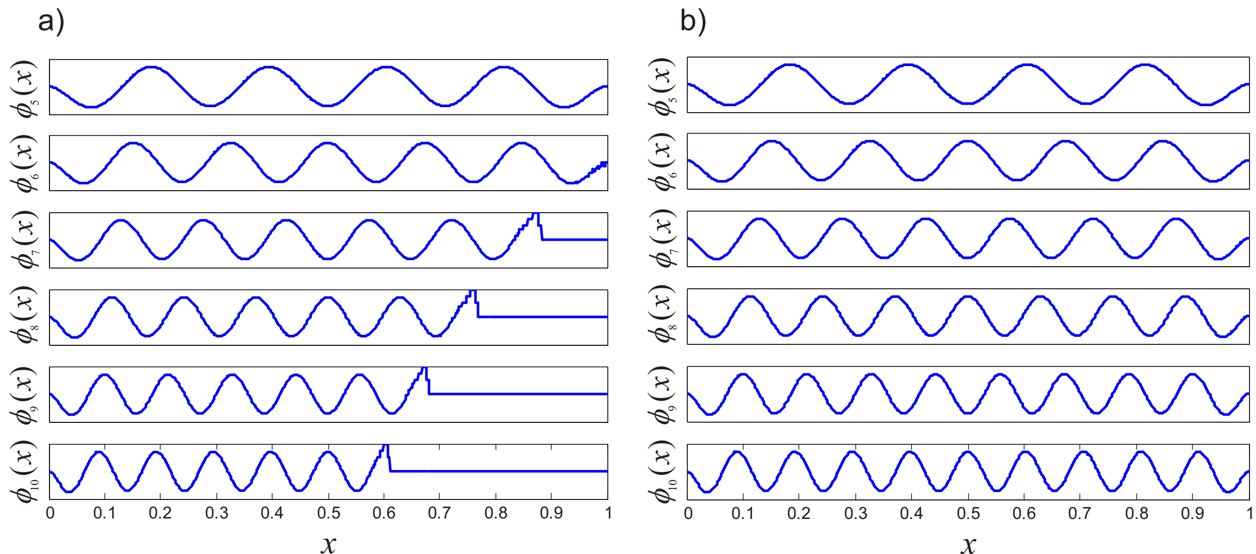

Fig. 4 Fifth to tenth symmetric mode shapes (*a*) obtained from the analytical expression given by Eq. (9) and (*b*) obtained by mirroring the left-half into the right-half of the modes. Note that the *y*-axis scale is arbitrary.

Downloaded From: http://computationalnonlinear.asmedigitalcollection.asme.org/ on 03/17/2013 Terms of Use: http://asme.org/terms

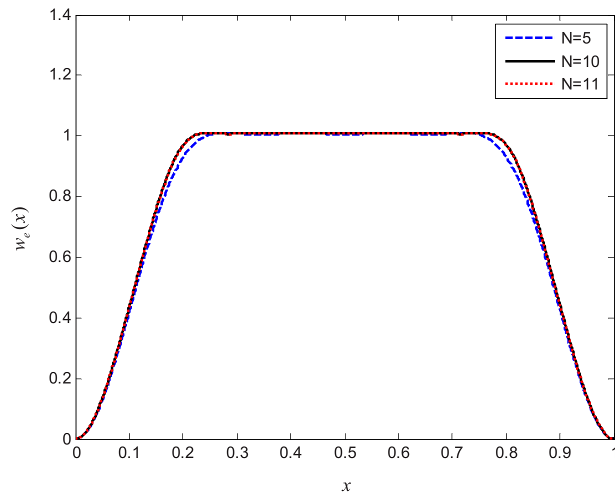

Fig. 6 Static deflection of the beam past pull-in using 5-mode, 10-mode, and 11-mode approximations at $V_{dc}=60$ V

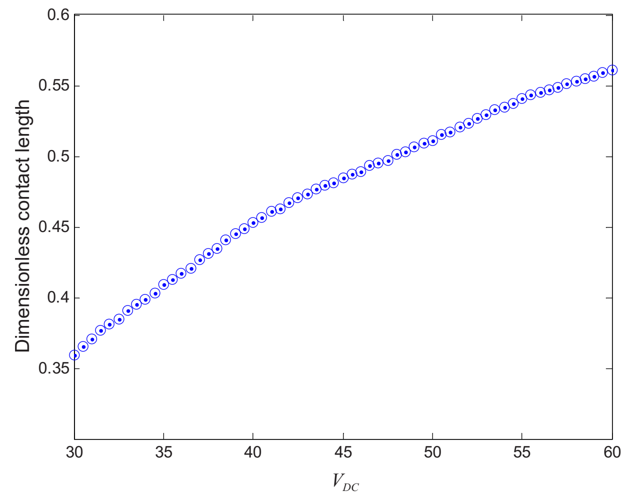

Fig. 8 The contact length of the beam with the substrate as a function of dc voltage

3.3 Static Response of the Beam. Figure 7 shows the midpoint deflection of the beam as a function of dc voltage.

The beam deflection increases with voltage and the rate of increase accelerates until pull-in occurs at $V=30$ V. The beam then jumps into contact and remains in contact with the substrate as the voltage is increased beyond pull-in. Figure 8 shows the contact length of the beam with the substrate as a function of dc voltage.

The increase in voltage causes an increase in the contact length. This relationship is almost linear until 40 V and then the rate of increase in the contact length with voltage drops down progressively as the voltage increases and saturates around 100 V.

3.4 Eigenvalue Problem. The natural frequencies of the beam motions around those static configurations are shown in Fig. 9. The natural frequency approaches zero as pull-in develops. After pull-in, the natural frequency increases as the beam comes in contact with the substrate. Contact with the substrate has a significant stiffening impact on the beam raising the natural frequency after contact to 4.97 times the natural frequency of the flat unactuated beam.

The first and second mode shapes of the beam superimposed on the static equilibrium are shown in Figs. 10 and 11 at selected values of the dc voltage beyond pull-in. The beam behaves as if it was two symmetric fixed-fixed beams stretching between the supports and the left and right ends of the contact length. For higher dc voltages, the peak values of the mode shapes shift toward the

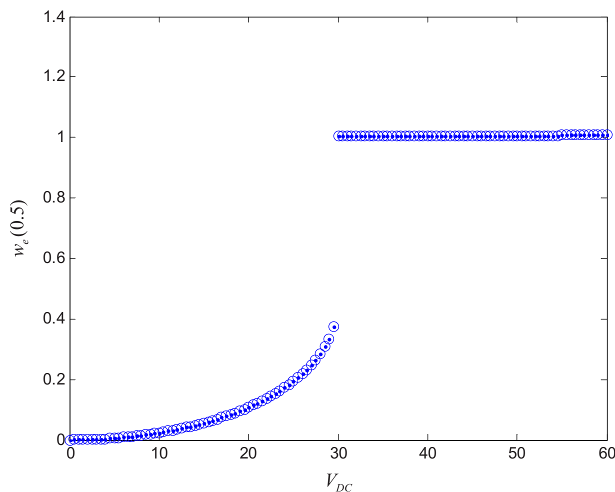

Fig. 7 Midpoint beam deflection as a function of dc voltage (V_{dc})

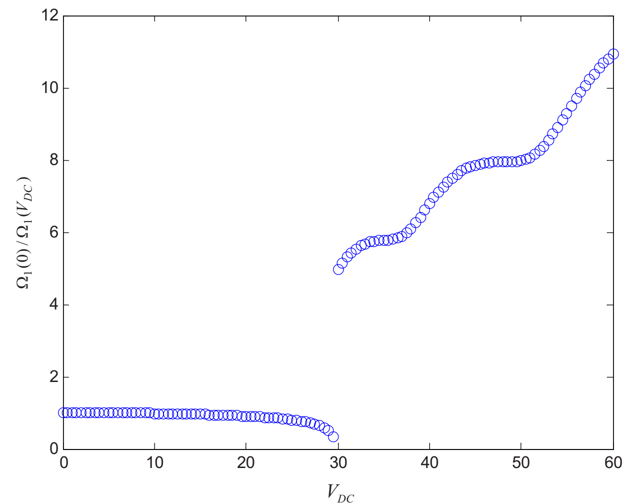

Fig. 9 Variation in natural frequency with dc voltage

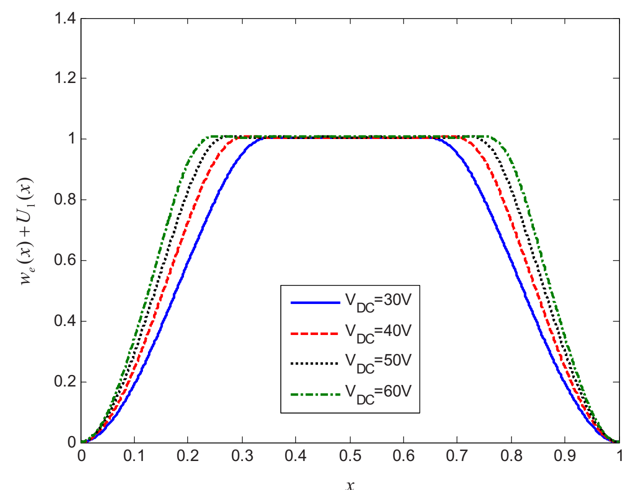

Fig. 10 Variation in the first mode shape with dc voltage

Downloaded From: http://computationalnonlinear.asmedigitalcollection.asme.org/ on 03/17/2013 Terms of Use: http://asme.org/terms

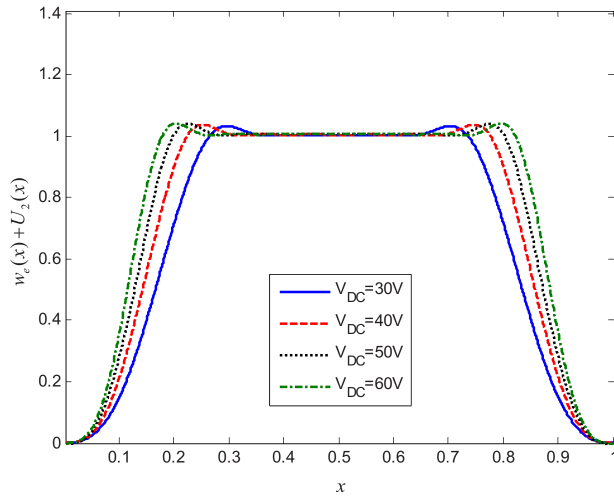

Fig. 11 Variation in the second mode shape with dc voltage

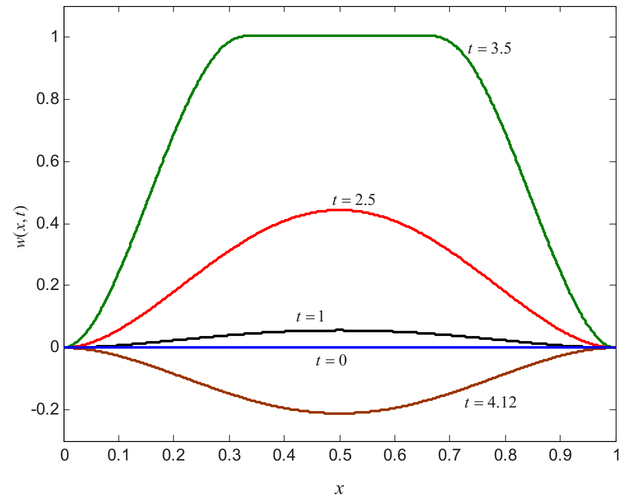

Fig. 13 Snapshots of the beam deformation

supports because the effective length of the "side beams" is shortening. However, the mode shapes appear to be similar for all the voltage values.

3.5 Dynamic Response of the Beam. We simulate the time history of a shunt switch with the properties listed in Table 1 and with three different values of the contact damping coefficient $\mu = 0.1$, 0.01, and 0.0001. The applied voltage waveform across the switch electrodes is

$$V(t) = \begin{cases} 15 & 0 < t \leq 2 \\ 30 & 2 < t \leq 4 \\ 0 & t > 4 \end{cases} \tag{18}$$

It represents the switch starting from rest at a flat position (ON-state) to settle at an intermediate position, closes and settles down to OFF-state, before releasing the beam to open the switch and return to the flat position. Figure 12 shows the midpoint deflection of the beam. The beam has settled down to the intermediate equilibrium position, as shown in Fig. 13, at $t=1$.

The switch starts closure from the intermediate position at $t=2$. The switching time from this position is found to be 1.32 units which is equivalent to 15.9 μs. At $t=4$, the voltage drops to zero and the beam pulls off the substrate, opening the switch under the influence of the mechanical restoring force. It overshoots the unactuated equilibrium position and settles down over time to that position. Figure 13 shows the snap shots of the beam at ON-state ($t=0$), at the intermediate position ($t=1$), during its evolution toward the substrate ($t=2.5$), at OFF-state ($t=3.5$), and at the extreme point of the rebound motion ($t=4.12$).

Figure 12(b) shows the oscillations of the beam midpoint during the initial phase of contact. It can be seen that the amplitude of oscillations is less than the contact deformation even for a very low value of the contact damping ($\mu=0.0001$); thus, the beam does not loose contact with the substrate and no contact bounce is observed. Bouncing motions were observed experimentally in series switches with point-contact [21–23]. The distributed nature of contact in our case, as opposed to switches with point-contact, seems to cause the smooth evolution of the contact zone, thus eliminating the bouncing. This would indicate that shunt switches have superior performance to series switches as far as bouncing contact is concerned.

4 Conclusions

We have developed a mathematical model for MEMS beams that is valid for motions encompassing pull-in. Convergence analysis shows that at least ten modes must be retained in the approximation to achieve convergent results. The contact length

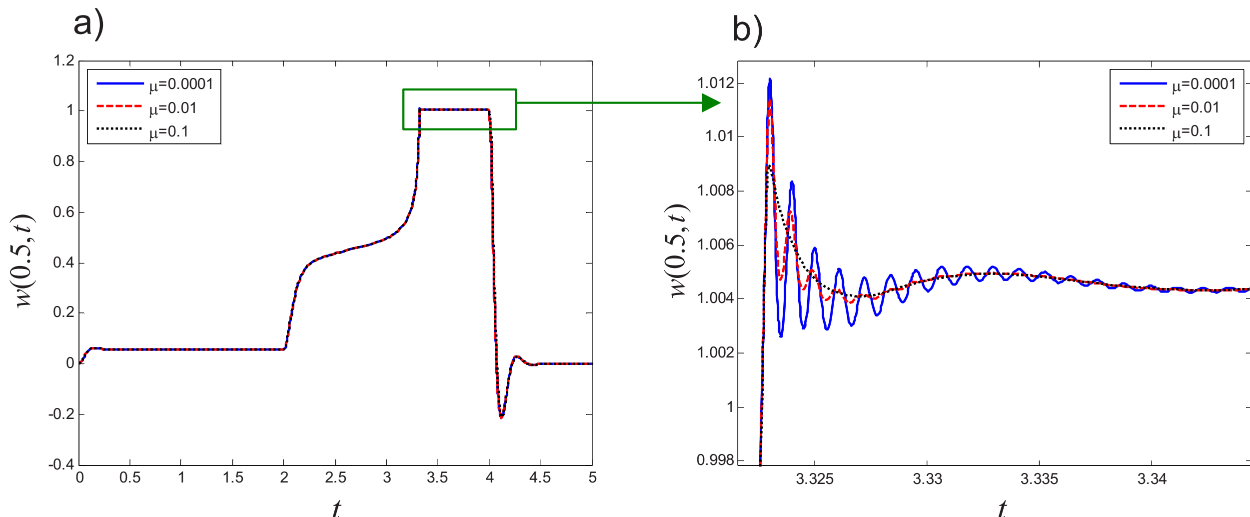

Fig. 12 (*a*) Response of the beam to the voltage waveform; (*b*) magnified view of the beam motion during contact

Downloaded From: http://computationalnonlinear.asmedigitalcollection.asme.org/ on 03/17/2013 Terms of Use: http://asme.org/terms

of the beam was found to initially increase linearly with dc voltage up to 40 V, then at a reduced rate until it saturates at 100 V as the contact length approaches two-thirds of the beam length.

The model can be used to simulate the complete dynamic response of micro-actuators during free-flight, impact, and contact with a substrate. It can be used to predict the mode shapes and natural frequencies of microbeams while in contact with a substrate, to simulate the motions of series and shunt switches, impact electrostatic actuators, and stiction-failure repair systems. We used our model to find the switching time of a shunt switch. We found that the switch did not demonstrate the bouncing contact reported for series switches with point-contact. We believe this to be the case due to the distributed nature of the contact zone evolution in shunt switches.

References

[1] Nayfeh, A. H., Younis, M. I., and Abdel-Rahman, E. M., 2007, "Dynamic Pull-In Phenomenon in MEMS Resonators," Nonlinear Dyn., **48**(1–2), pp. 153–163.

[2] Younis, M., Abdel-Rahman, E., and Nayfeh, A., 2003, "A Reduced-Order Model for Electrically Actuated Microbeam-Based MEMS," J. Microelectromech. Syst., **12**(5), pp. 672–680.

[3] Gupta, R., Hung, E., Yang, Y., Ananthasuresh, G., and Senturia, S., 1996, "Pull-In Dynamics of Electrostatically-Actuated Beams," Proceedings of the Solid-State Sensor and Actuator Workshop.

[4] Nielson, G., and Barbastathis, G., 2006, "Dynamic Pull-In of Parallel-Plate and Torsional Electrostatic MEMS Actuators," J. Microelectromech. Syst., **15**(4), pp. 811–821.

[5] Fargas-Marques, A., and Shkel, A., 2005, "On Electrostatic Actuation Beyond Snapping Condition," Proceedings of the IEEE Sensors, Irvine, CA, pp. 600–603.

[6] Fargas-Marques, A., Castelló, R., and Shkel, A., 2005, "Modelling the Electrostatic Actuation of MEMS: State of the Art 2005," Technical Report No. IOC-DT-P-2005-18.

[7] Elata, D., and Bamberger, H., 2006, "On the Dynamic Pull-In of Electrostatic Actuators With Multiple Degrees of Freedom and Multiple Voltage Sources," J. Microelectromech. Syst., **15**(1), pp. 131–140.

[8] Nayfeh, A. H., and Younis, M. I., 2005, "Dynamics of MEMS Resonators Under Superharmonic and Subharmonic Excitations," J. Micromech. Microeng., **15**, pp. 1840–1847.

[9] Savkar, A., and Murphy, K., 2010, "The Evolution of Stiction Repair for Microelectromechanical System Cantilevers Using Periodic Excitation," J. Sound Vib., **329**(2), pp. 189–201.

[10] Savkar, A., and Murphy, K., 2008, "Mechanics of the Dynamic Release Process for Stiction Failed Microcantilever Beams Using Structural Vibrations," Proc. SPIE, **6884**, p. 68840A.

[11] Savkar, A., Murphy, K., Leseman, Z., Mackin, T., and Begley, M., 2007, "On the Use of Structural Vibrations to Release Stiction Failed MEMS," J. Microelectromech. Syst., **16**(1), pp. 163–173.

[12] Gorthi, S., Mohanty, A., and Chatterjee, A., 2006, "Cantilever Beam Electrostatic MEMS Actuators Beyond Pull-In," J. Micromech. Microeng., **16**, pp. 1800–1810.

[13] Bienstman, J., Vandewalle, J., and Puers, R., 1998, "The Autonomous Impact Resonator: A New Operating Principle for a Silicon Resonant Strain Gauge," Sens. Actuators, A, **66**(1–3), pp. 40–49.

[14] Gilardi, G., and Sharf, I., 2002, "Literature Survey of Contact Dynamics Modelling," Mech. Mach. Theory, **37**(10), pp. 1213–1239.

[15] Hunt, K., and Crossley, F., 1975, "Coefficient of Restitution Interpreted as Damping in Vibroimpact," ASME J. Appl. Mech., **42**(2), pp. 440–445.

[16] Gonthier, Y., McPhee, J., Lange, C., and Piedboeuf, J., 2004, "A Regularized Contact Model With Asymmetric Damping and Dwell-Time Dependent Friction," Multibody Syst. Dyn., **11**(3), pp. 209–233.

[17] Marhefka, D., and Orin, D., 1999, "A Compliant Contact Model With Nonlinear Damping for Simulation Ofrobotic Systems," IEEE Trans. Syst. Man Cybern., Part A. Syst. Humans, **29**(6), pp. 566–572.

[18] Nayfeh, A., and Mook, D., 1995, *Nonlinear Oscillations*, Wiley, New York.

[19] Legtenberg, R., and Tilmans, H., 1994, "Electrostatically Driven Vacuum-Encapsulated Polysilicon Resonators Part I. Design and Fabrication," Sens. Actuators, A, **45**(1), pp. 57–66.

[20] Gonçalves, P., Brennan, M., and Elliott, S., 2007, "Numerical Evaluation of High-Order Modes of Vibration in Uniform Euler–Bernoulli Beams," J. Sound Vib., **301**(3–5), pp. 1035–1039.

[21] McCarthy, B., Adams, G. G., McGruer, N. E., and Potter, D., 2002, "A Dynamic Model, Including Contact Bounce, of an Electrostatically Actuated Microswitch," J. Microelectromech. Syst., **11**(3), pp. 276–283.

[22] Sumali, H., Massad, J., Czaplewski, D., and Dyck, C., 2007, "Waveform Design for Pulse-and-Hold Electrostatic Actuation in MEMS," Sens. Actuators, A, **134**(1), pp. 213–220.

[23] Blecke, J. C., Epp, D. S., Sumali, H., and Parker, G. G., 2009, "A Simple Learning Control to Eliminate RF-MEMS Switch Bounce," J. Microelectromech. Syst., **18**(2), pp. 458–465.

Downloaded From: http://computationalnonlinear.asmedigitalcollection.asme.org/ on 03/17/2013 Terms of Use: http://asme.org/terms